Journal of ELECTRONIC MATERIALS, Vol. 43, No. 2, 2014
DOI: 10.1007/s11664-013-2858-7
© 2013 TMS

Numerical Modeling of Multimaterial Thermoelectric Devices Under Static and Cyclic Thermal Loading

JEFFREY W. FERGUS,[1,3] KIRK YERKES,[2] and KEVIN YOST[2]

1.—Materials Research and Education Center, Auburn University, Auburn, AL 36849, USA. 2.—Aerospace Systems Directorate, Wright–Patterson Air Force Research Laboratory, WPAFB, OH 45433, USA. 3.—e-mail: jwfergus@eng.auburn.edu

Selection of materials for thermoelectric devices is generally based on a figure of merit that is a function of the Seebeck coefficient, electrical conductivity, and thermal conductivity. While this figure of merit is a useful metric for comparing materials, the relative importance of the constituent properties depends on the particular application and conditions. In addition, multiple materials can be used together to improve the performance or extend the operating range, and determining the performance of such multimaterial combinations requires analysis beyond simply averaging the properties of the constituent materials. In this paper, finite-element numerical simulations under static and cyclic thermal loadings are used to investigate how device performance can be improved by judicious location of the different materials within the device. The results show that the performance of a device with two different materials can be better than that of either of the individual materials. The greatest improvement in performance occurs with cyclic heating, where the overall performance is strongly influenced by the behavior under transient conditions during heating and cooling.

Key words: Thermoelectric figure of merit, cascaded thermoelectric devices, multistage thermoelectric elements, segmented thermoelectric elements

INTRODUCTION

Thermoelectric energy conversion provides a means for production of electric power from waste heat. Thermoelectric generators are solid state and require no moving parts, which leads to good durability and is particularly attractive for applications where maintenance or repair is difficult. A major disadvantage of thermoelectric generators is that the efficiency of energy conversion is low. However, in applications where the amount of waste heat is high and/or the electric power demands are low, such low efficiency may be acceptable; for example, thermoelectric generators can harvest electrical energy from waste heat in power plants[1] or solid-oxide fuel cells.[2] If the amount of power needed is small, such as for low-power sensors, thermoelectric generators may also be useful in lower-temperature applications, such as mounting in the ground[3] or in the wall of a building.[4] The interest in thermoelectric energy conversion in automotive applications is growing, since there is a significant amount of waste heat in the exhaust gas or engine coolant,[5,6] and the increased number of electronic devices for control, safety, and comfort, as well as the increased use of electric motors for propulsion in hybrid vehicles, have increased the value of harvesting electric power from waste heat. The durability associated with the solid-state design of thermoelectric generators is attractive for automotive as well as aerospace applications.[7] Modeling of thermoelectric conversion systems is important for improving the effectiveness of thermoelectric energy conversion at the device[8,9] and supporting system levels.[10–12] In this paper, modeling is used to understand the effect of materials properties on performance.

(Received August 26, 2013; accepted October 8, 2013; published online November 26, 2013)

MATERIALS SELECTION

The parameter typically used to select materials for thermoelectric devices is the figure of merit, ZT,

$$ZT = \left(\frac{\alpha^2\sigma}{\lambda}\right)T, \quad (1)$$

where α is the Seebeck coefficient, σ is the electrical conductivity, λ is the thermal conductivity, and T is the temperature. Although the figure of merit includes the properties contributing to the thermoelectric performance, the relative importance of these properties depends on the particular operational parameters; For example, introduction of thermal interfaces has been shown to increase the importance of the thermal conductivity relative to the Seebeck coefficient for the power and efficiency of the device.[13] The thermoelectric properties of materials vary with temperature, so the selection of materials depends on the operating temperature. In some cases, the operating temperature range exceeds that for satisfactory performance or stability of a particular material, so multiple materials can be used in cascaded or segmented thermoelectric generators.[14] In addition to the performance of the individual materials, the similarity of the properties among the materials used affects the performance of the device, so the compatibility of the materials must also be considered.[15,16]

The use of multiple materials most commonly involves selecting materials for the hot or cold side of the device based on their respective figures of merit in those temperature ranges; For example, bismuth telluride is the most commonly used thermoelectric material, but is not suitable for use at high temperatures, so it is combined with other materials with superior high-temperature properties. Lead telluride has better high-temperature thermoelectric properties than bismuth telluride and has been used on the hot side of both the n-type[17,18] and p-type[19] legs of segmented thermoelectric devices. Other materials that have been used for the hot side of the n-type leg include intermetallic compounds [$CoSb_3$,[20,21] (Zr,Hf)CoSb half-Heusler phases,[22] and Mg_2Si[23]] and oxides (zinc oxide[24] and strontium titanate[24]). Materials used for the hot side of the p-type leg of segmented elements include TAGS [$(AgSbTe_2)_{1-x}(GeTe)_x$],[17] LASTT ($Ag_{0.5}Pb_6Sn_2Sb_{0.2}Te_{10}$),[18] $CeFe_4Sb_{12}$,[20,21] Zn_4Sb_3,[23] and half-Heusler (Zr,Hf)CoSb.[22] Oxides, including titanium oxide,[24] $Na_xCo_2O_4$,[24] and $Ca_3Co_4O_9$,[25] have also been used for the hot side of the p-type leg of such devices. While the use of multiple materials provides improved performance, additional stresses can be generated due to differences in thermal expansion between the materials.[26] Such stresses can be minimized by using materials with graded properties, which has been investigated for thermoelectric devices.[27]

The focus in selecting materials for thermoelectric applications is often on the properties that determine the figure of merit in Eq. 1, but other properties are important for the performance and durability of thermoelectric devices. The magnitudes of the thermal stresses depend on the relative magnitudes of the coefficients of thermal expansion, and the response of the material to those stresses depends on the mechanical properties. However, the objective of this study is to determine the relative importance of the thermal and electrical conductivity for the performance of thermoelectric devices under transient heating and cooling conditions, so, although important for device design, mechanical stresses were not considered in this analysis. Such analysis would certainly be needed for the implementation of devices, but lies beyond the scope of this paper.

To focus on the trade-off between the electrical and thermal conductivity, model materials were created so that these two properties could be isolated. The Seebeck coefficients, electrical resistivities, and thermal conductivities of the model materials were based on a recently published compilation of thermoelectric properties of ceramic materials.[28] All model materials had the same Seebeck coefficient, as shown in Fig. 1a. Materials with three different electrical conductivities were used, as shown in Fig. 1b. Material 1 has a high electrical conductivity, which is based on the properties of $SrTiO_3$ and ZnO. Materials 2 and 3 both have low electrical conductivities, but different temperature dependences. The conductivity of material 2 increases with increasing temperature, as is typical of the small-polaron conduction mechanism, while the conductivity of material 3 decreases with temperature, as for metallic-type conduction. The thermal conductivities of the model materials, shown in Fig. 1c, were calculated from the electrical conductivities to maintain the same figure of merit, which, as shown in Fig. 1d, is in the middle range of oxide materials reported in the literature. The heat capacities were similarly based on values reports in the literature for $SrTiO_3$,[29] ZnO,[30] $CaMnO_3$,[31] and $Ca_3Co_4O_9$[32] and are shown in Fig. 1e.

NUMERICAL MODEL

Numerical modeling was performed using the thermoelectric module of ANSYS software.[33] The governing equations are based on analysis of heat flow

$$\rho C\frac{\partial T}{\partial t} + \nabla\cdot\mathbf{q} = \dot{q}, \quad (2)$$

and continuity of electric charge

$$\nabla\cdot\left(\mathbf{J} + \frac{\partial \mathbf{D}}{\partial t}\right) = 0, \quad (3)$$

using thermoelectric constitutive equations

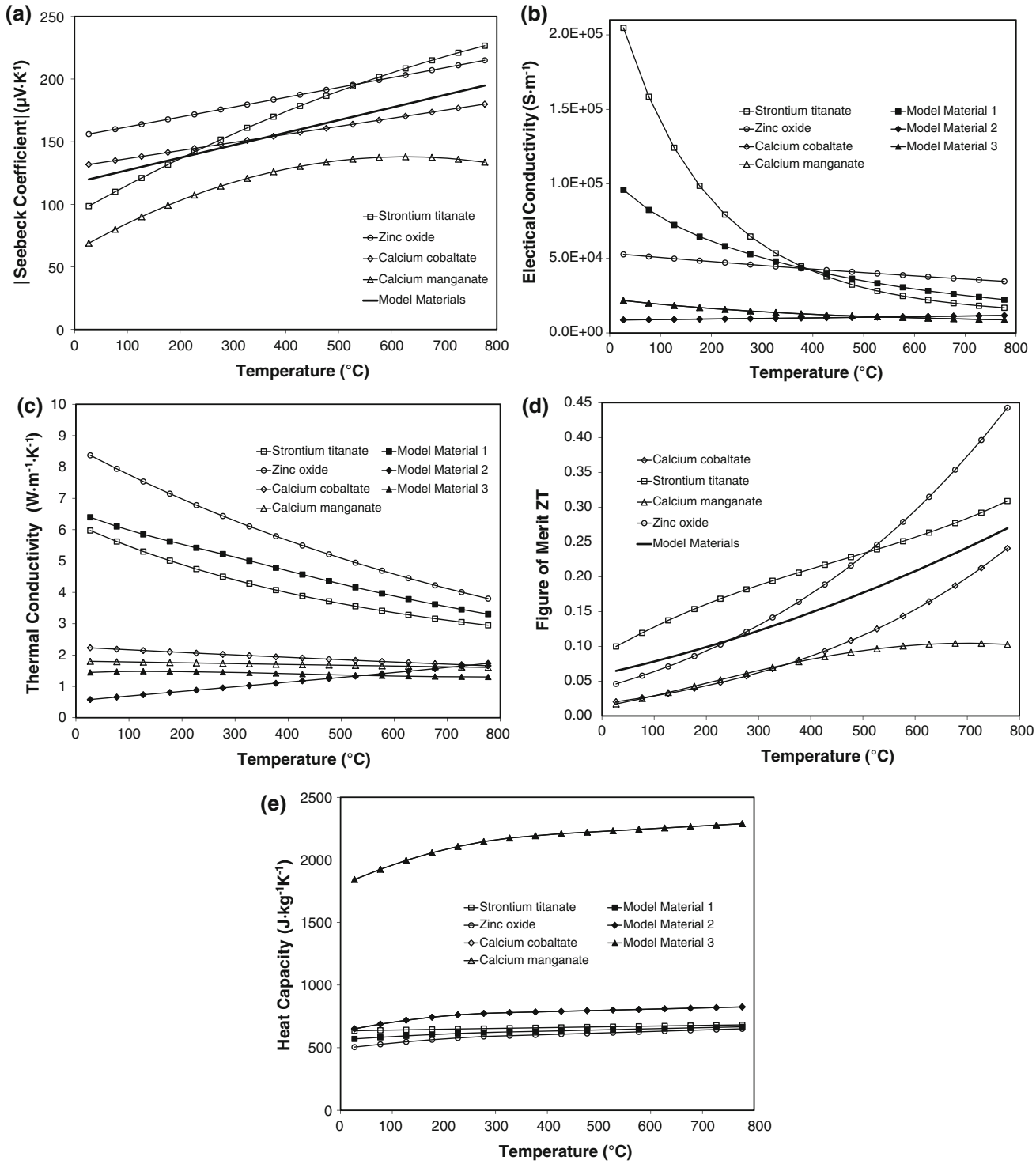

Fig. 1. Properties of model materials: (a) Seebeck coefficient, (b) electrical conductivity, (c) thermal conductivity, (d) figure of merit, and (e) heat capacity. Values from the literature[28–32] are shown for comparison.

$$\mathbf{q} = [\pi] \cdot \mathbf{J} - [\lambda] \cdot \nabla T, \tag{4}$$

$$\mathbf{J} = [\sigma] \cdot (\mathbf{E} - [\alpha] \cdot \nabla T), \tag{5}$$

where ρ is the density (kg m^{-3}), C is the specific heat capacity (J kg^{-1} K^{-1}), T is the temperature, $\dot{q}$ is the heat generation rate per unit volume (W m^{-3}), $\mathbf{q}$ is the heat flux vector (W m^{-2}), $\mathbf{J}$ is the electric current density vector (A m^{-2}), $\mathbf{E}$ is the

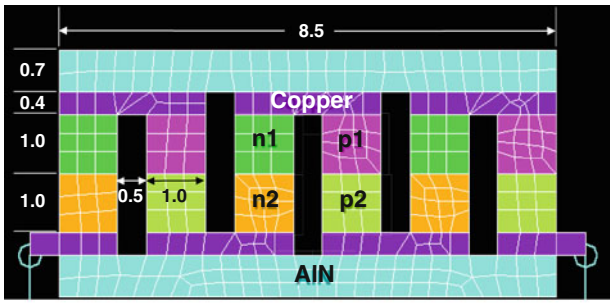

Fig. 2. ANSYS model; dimensions in mm.

Table I. Model materials for simulations

	Material Properties	
Designation	**Hot (*n*1, *p*1)**	**Cold (*n*2, *p*2)**
Material 11 or material 1	1	1
Material 22 or material 2	2	2
Material 33 or material 3	3	3
Material 12	1	2
Material 21	2	1
Material 13	1	3
Material 31	3	1

	Properties	
	Thermoelectric	**Heat Capacity**
Material 11, high C_p	1	3
Material 22, high C_p	2	3
Material 33, low C_p	3	2

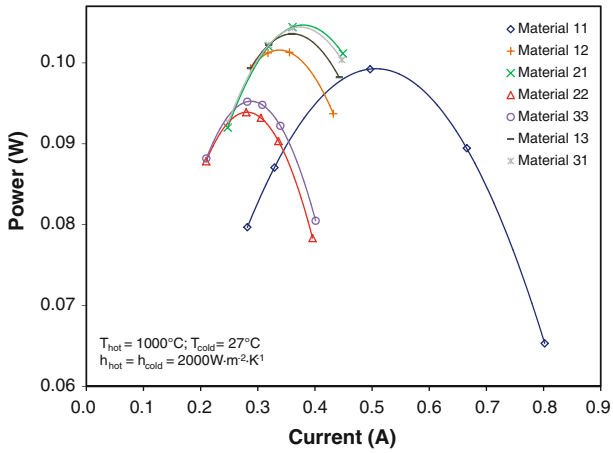

Fig. 3. Effect of current (load) on output power.

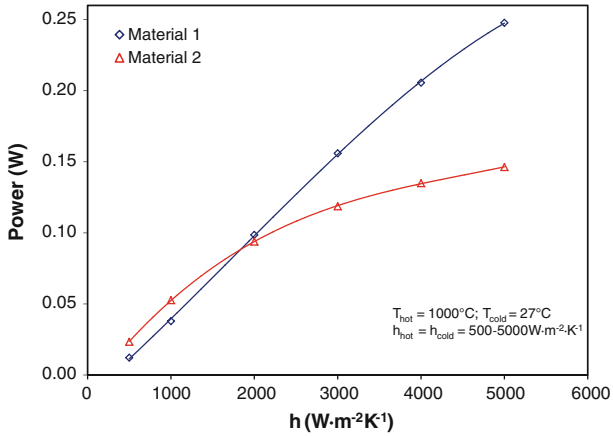

Fig. 4. Effect of heat transfer coefficient on power.

electric field intensity vector (V m^{-1}), [λ] is the thermal conductivity matrix (W m^{-1} K^{-1}), [σ] is the electrical conductivity matrix (S m^{-1}), [α] is the Seebeck coefficient matrix (V K^{-1}), and [π] = T[α] is the Peltier coefficient matrix (V).

The model used consists of three *p*–*n* thermoelectric pairs connected in series, as shown in Fig. 2. Each leg of the module has two sections so that two different materials can be used. The materials used in the simulations are summarized in Table I. The first symbol indicates the material at the hot side (*n*1, *p*1 in Fig. 2), and the second symbol indicates the material used for the cold side (*n*2, *p*2 in Fig. 2). In addition, the effect of the heat capacity was evaluated by performing additional simulations using a high heat capacity for materials 1 and 2 and a low heat capacity for material 3.

The mesh independence of the results was verified by performing simulations for three different materials using three different mesh sizes. The results were indistinguishable on the plots used to analyze the results. The maximum temperature difference between any of the 6000 temperatures used from these three simulations (3 simulations × 1000 time intervals/simulation × 2 temperatures/time interval) for the mesh shown in Fig. 2 (1120 nodes) and either finer (1680 nodes) or coarser (497 nodes) meshes was 0.4°C. The agreement in the output voltage was even more consistent in that the maximum difference in voltage between any of the 3000 voltages from these three simulations was 0.2 μV.

The thermoelectric module is connected to a load resistance, the magnitude of which was used to control the current, and thus the power, generated by the device. Because of differences in electrical conductivity, the load resistance and current for maximum power differed among the materials as shown in Fig. 3. The load resistance used for materials 2 and 3 (1.2 Ω) was three times that for material 1 (0.4 Ω). For combinations of materials 1 and 2 or 1 and 3, the load resistance was halfway between these values (i.e., 0.8 Ω).

The thermal load was applied using convective heating and cooling on the AlN surfaces. In such cases, the relative importance of the electrical and thermal conductivity depends on the heat transfer

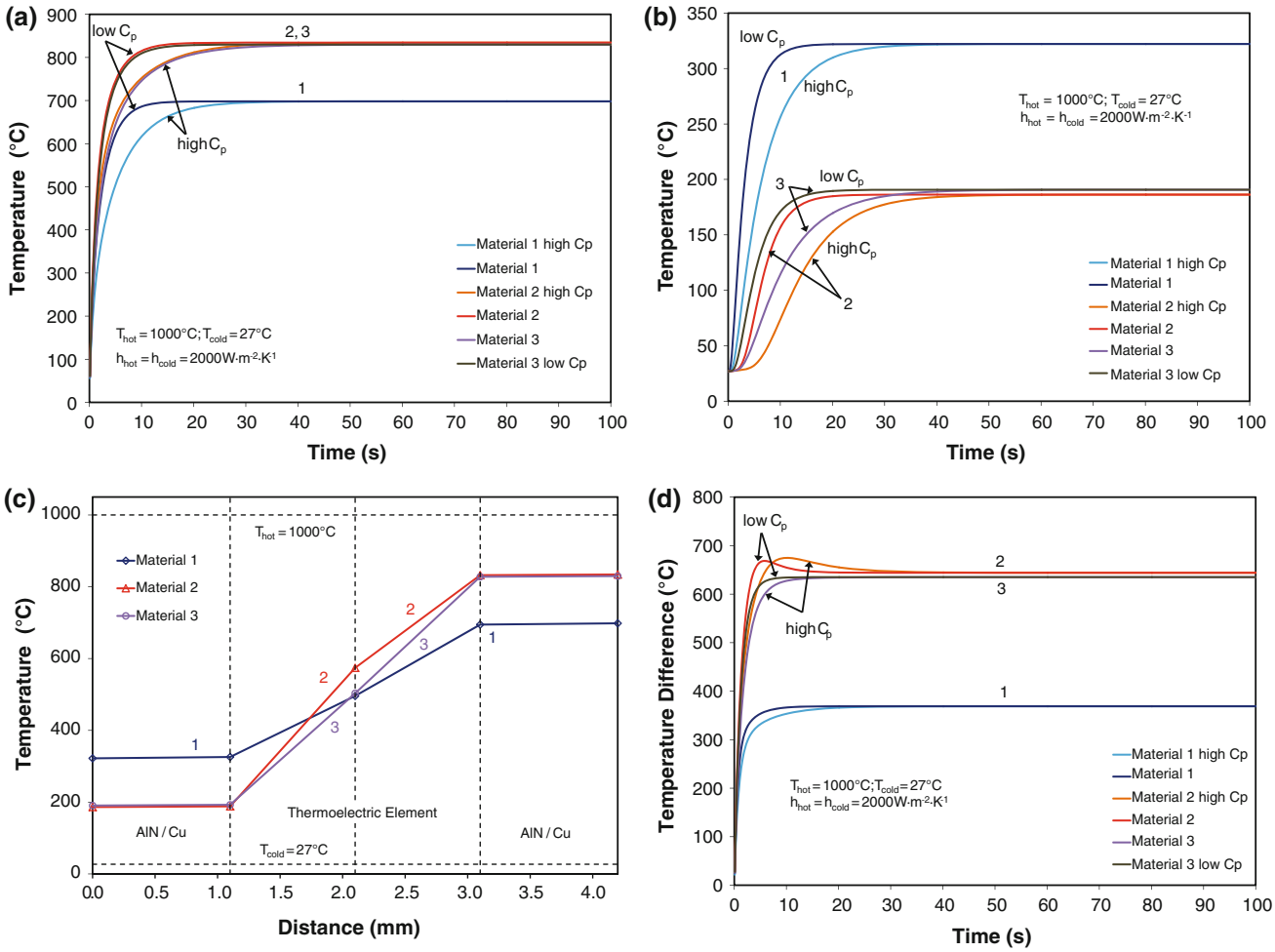

Fig. 5. Temperatures for step to 1000°C: (a) hot side, (b) cold side, (c) gradient, and (d) temperature difference.

coefficient as shown in Fig. 4. For high heat transfer coefficients, the material with higher electrical conductivity (i.e., material 1) generates more power because of the low electrical resistance. However, for low heat transfer coefficients, the material with low thermal conductivity (i.e., material 2) generates more power because a larger temperature gradient, and thus larger output voltage, is developed. To focus on material placement, a heat transfer coefficient for which the power of the two materials is similar was used. For all simulations, the bulk temperature on the cold side was 27°C and the heat transfer coefficient was 2000 W m^{-2} K^{-1}. A heat transfer coefficient of 2000 W m^{-2} K^{-1} was also used on the hot side, but the bulk temperature on the hot side was either stepped to 1000°C and held for 100 s or cycled between 200°C and 1000°C with cycle durations of 1 s to 100 s.

RESULTS AND DISCUSSION

The focus of this study was on the performance of multimaterial thermoelectric elements in transient conditions. However, to demonstrate the performance during initial heating and at steady state, results for single- and multimaterial thermoelectric elements in response to a single step function are presented first.

Single Temperature Step—Single Material

The hot and cold temperatures in response to a step increase in temperature to 1000°C are shown in Fig. 5a and b, respectively. Since the heat capacity of material 3 is considerably higher than those of materials 1 and 2, additional simulations using different heat capacities were performed. In particular, materials 1 and 2 with the heat capacity of material 3 (high C_p) and material 3 with the heat capacity of material 2 (low C_p) were used. The delay in heating associated with a high heat capacity affects the time taken to reach the steady-state temperatures, but not the steady-state values, and thus may be important in transient or thermal cycling conditions, whereas the low thermal conductivity affects both the heating times and the steady-state temperatures. The temperature distribution through the device after steady state has

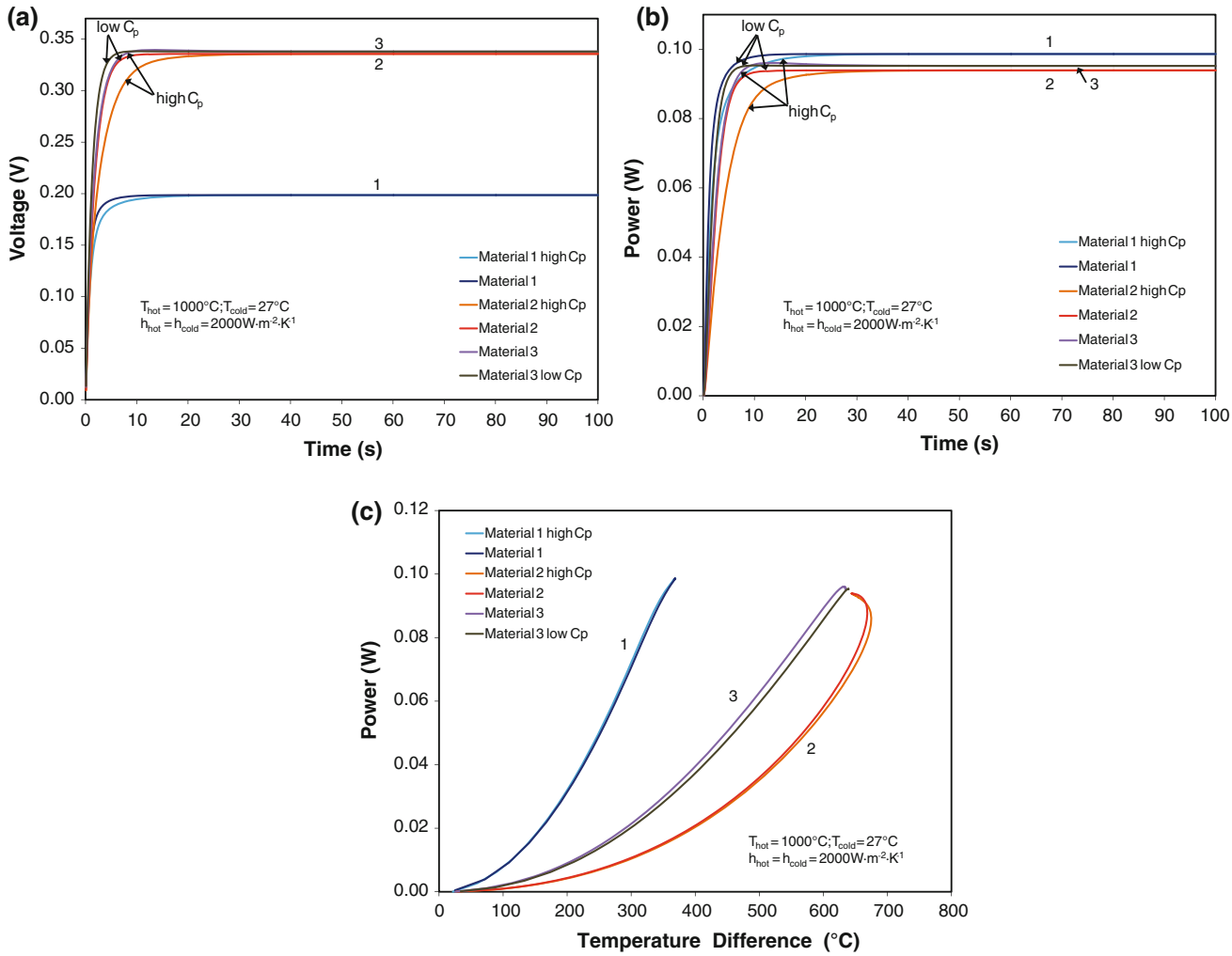

Fig. 6. Device output for step to 1000°C: (a) voltage, (b) power, and (c) power versus temperature difference.

been reached (i.e., 100 s) is shown in Fig. 5c. Although the average thermal conductivities of materials 2 and 3 are similar, the temperature differences across the device are different. The thermal conductivity of material 2 increases with increasing temperature, so the temperature gradient is shallower in the high-temperature section. In some cases (specifically, material 2), but not all, a peak in the temperature difference between the hot and cold sides occurs during heating, as shown in Fig. 5d.

The temperature difference across the device generates a voltage according to the Seebeck effect, so the voltage is expected to follow a trend similar to that of the temperature difference. Figure 6a shows that the trend in voltage is generally the same as the trend in temperature difference, but there is little or no peak in voltage. The dampening of this peak is discussed in more detail in the next section. Although the high thermal gradient of material 1 leads to a small temperature difference across the device, the high electrical conductivity leads to a higher current which increases power, such that the output powers for all three materials are similar as shown in Fig. 6b. The amount of power generated for a given temperature difference, shown in Fig. 6c, is higher for the material with higher electrical conductivity (material 1), since the beneficial effect of low thermal conductivity in increasing the temperature gradient is eliminated by comparing the power at a fixed temperature difference.

Single Temperature Step—Two Materials

Simulations were performed with a combination of a high-conductivity material (material 1) and a low-conductivity material (material 2 or 3). Of particular interest are the combinations including material 2, all of which have a peak in the temperature difference across the device, as shown in Fig. 7a. Material 21 is of particular interest since this peak is maintained in the voltage (Fig. 7b) and in the output power (Fig. 7c). The output power for material 12, which has the same materials as material 21 but with material 1 on the hot rather

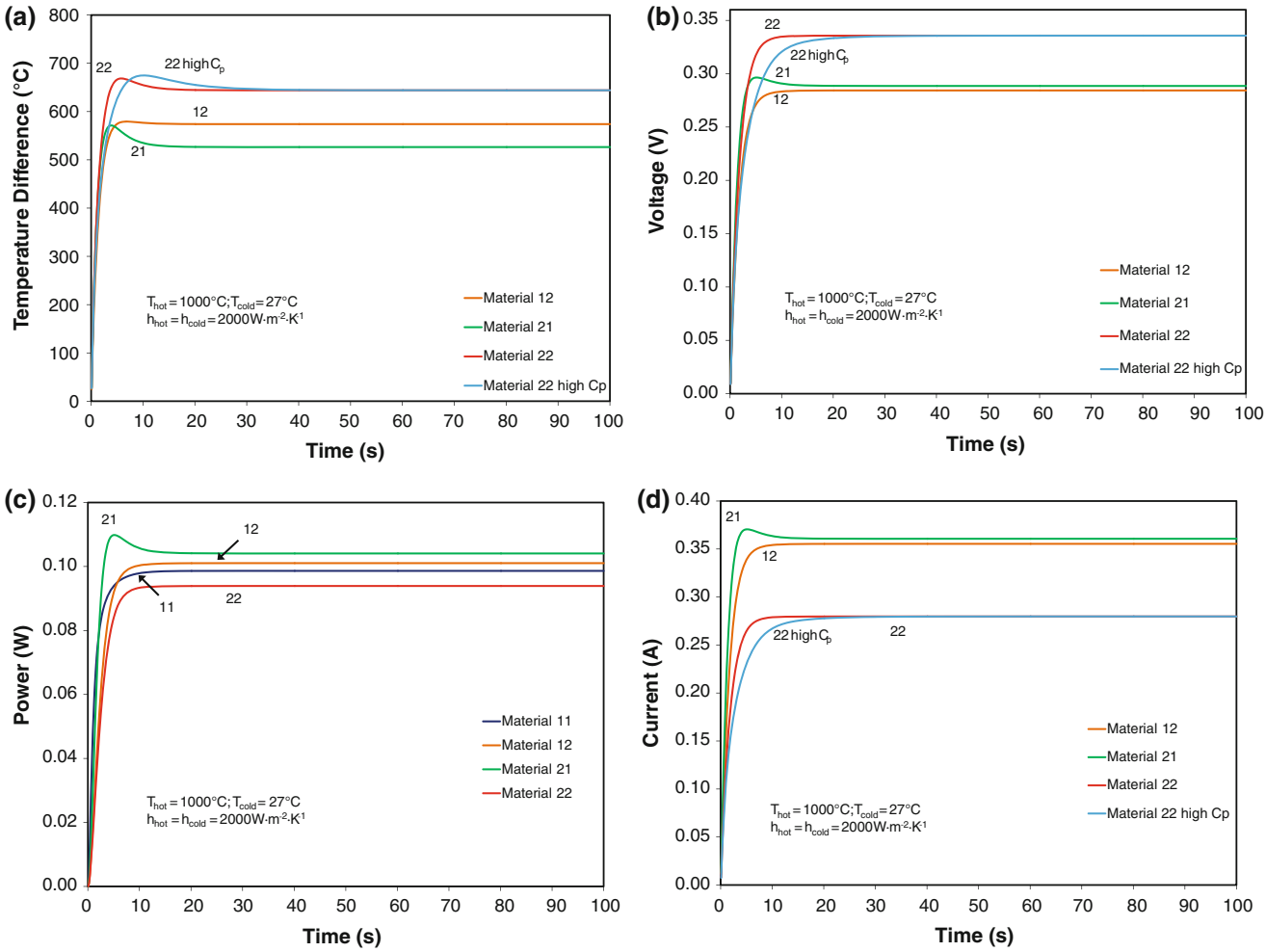

Fig. 7. Output of devices with material 2 for step to 1000°C: (a) temperature difference, (b) voltage, (c) power, and (d) current.

than cold side, does not show this peak. This peak in power is of particular interest since the performance during and shortly after heating is important for transient heating conditions.

One of the reasons for the diminishing of the peak in voltage is the decrease of the Seebeck coefficient with temperature (Fig. 1a) such that the voltage for a given temperature difference is smaller. However, all materials have the same Seebeck coefficient, so the differences between different materials are due to other properties. One of the factors influencing the presence or absence of a peak in the voltage, and thus power, is the current, since, for a given temperature difference across a thermoelectric material, the voltage decreases with increasing current. Figure 7d compares the currents for the elements with material 2 and shows that the current for material 21 also exhibits a peak.

The difference in the behavior of materials 12 and 21 appears to be due to the differences in the temperature dependence of the conductivity. The resistance of material 1 increases with increasing temperature, while the resistance of material 2 decreases with increasing temperature. To evaluate the effect of this difference, the average temperatures of the two sections of the thermoelectric device were used to determine the contributions of the two sections to the overall resistance. The results in Fig. 8a show that the temperature dependence is dominated by the material on the hot side, so that the resistance of material 21 decreases with temperature during heating (i.e., material 2 dominates). The impact of this is shown in Fig. 8b, where for material 21 the resistance decreases before the peak in temperature difference and then increases slightly after the peak, whereas the rate of increase in resistance for material 12 decreases after the peak in temperature difference. The decreasing rate of increase in resistance leads to a decreasing rate of decrease in current, so the decrease in voltage is diminished for material 12. The difference between the change in current after heating is evident in Fig. 7d, which shows the current for material 12 leveling off as the maximum temperature is reached, while the current for material 21 decreases after the peak in temperature.

Simulations performed using materials 1 and 3 showed that a peak in power was not present for

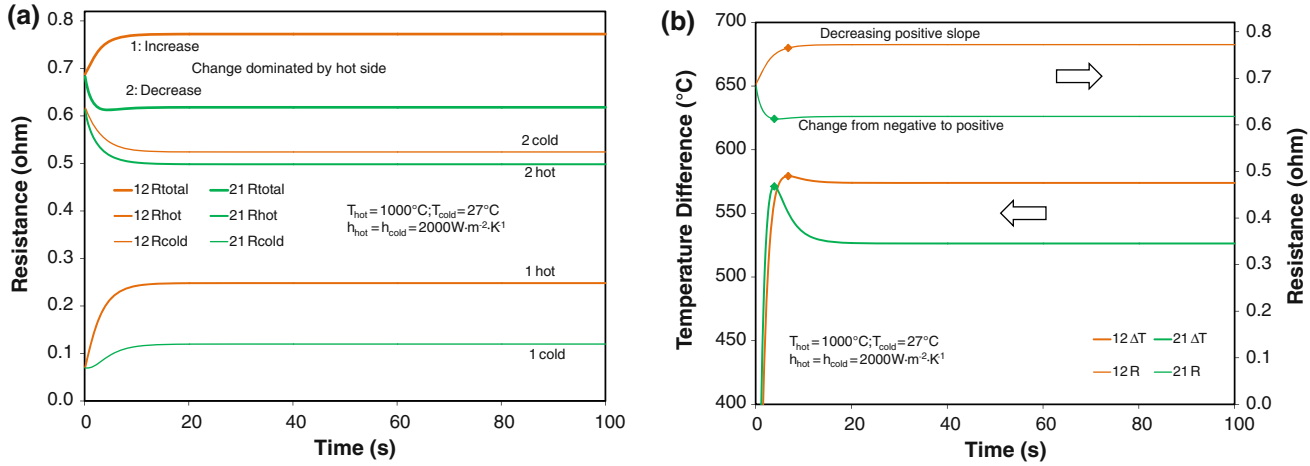

Fig. 8. Electrical resistances of devices with materials 12 and 21 for step to 1000°C: (a) contributions from hot/cold side, and (b) correlation with temperature difference.

any combination (i.e., materials 33, 13 or 31), and that the difference between materials 13 and 31 was very small. However, the powers for both combinations of materials 1 and 3 (i.e., materials 13 or 31) were higher than that for either material 1 or 3 alone.

Temperature Cycling

To evaluate the performance in transient conditions, cyclic heating/cooling between 1000°C and 200°C with cycle duration of 1 s, 2 s, 5 s, 10 s, 20 s, 50 s, and 100 s was applied. A few examples of the power output under cyclic heating/cooling are shown in Fig. 9. The 100-s cycle (Fig. 9a) is essentially the same as the step to 1000°C, except that the temperature change during the first cycle is different since the device is heated from room temperature. For the 10-s cycle (Fig. 9b), the power is just reaching the steady-state value when the temperature is decreased. As for the 100-s cycle, the power in the first cycle is slightly different than in subsequent cycles, but eventually the cycles are repeatable. The peak in power for material 21 appears more prominently for the 10-s cycle than for the 100-s cycle, since the power has not decreased to the steady-state value before the temperature at the hot side of the device is decreased. For the 1-s cycle (Fig. 9c), the power is lower since the device does not have time to heat up and it takes a few cycles to reach repeatable cycles, but the cycles do become repeatable.

To investigate the effect of cycle length, the average power for each cycle was determined. In some cases power was generated when the hot temperature was 200°C, so the average power included the entire cycle (i.e., the times at both 200°C and 1000°C). As an example, a summary of the power for each cycle for material 21 is shown in Fig. 10. For all cycle lengths, the average power reaches a constant value, which is expected, since the cycles become repeatable as shown in Fig. 9. For comparison, the power at the end (100 s) of the step to 1000°C is represented by a broken line. The steady-state power is divided by two since this does not include the low-temperature part of the cycle that was used for the results with temperature cycling. The constant value for the 100-s cycles is slightly higher than one-half of the steady-state power at 100 s, because some power is generated when the hot temperature is 200°C, which is not included in the steady-state value of power.

To compare the different materials, the average power for the last cycle for each cycle length was used. Although the time for the last cycle is not the same for all cycle lengths, the average power reached a constant value in all cases. Figure 11a shows that all materials exhibited the same general increase in power with cycle length since the temperature has more time to increase for the longer cycles. The material with the highest power was material 21, and the difference is particularly notable for the short time periods; For example, for cycle lengths from 5 s to 20 s, the average power for material 21 is 8% to 9% higher than that for material 11. Thus, adding material 2, which by itself generates less power than material 1, to material 1 leads to an increase in power. The power generated by material 12 is also greater than that generated by material 11, but only at longer cycles, and the difference is not as large as that between materials 11 and 21.

The average heat entering the device during the last cycle as a function of cycle length is shown in Fig. 11b. Like the power output, the heat flux reaches a constant value for each material. The heat flux for material 1 is higher than those for materials 2 and 3 due to the higher thermal conductivity of material 1. As expected, the heat fluxes for materials 12 and 21 lie between those for materials 1 and 2, but material 21 has a higher heat flux than

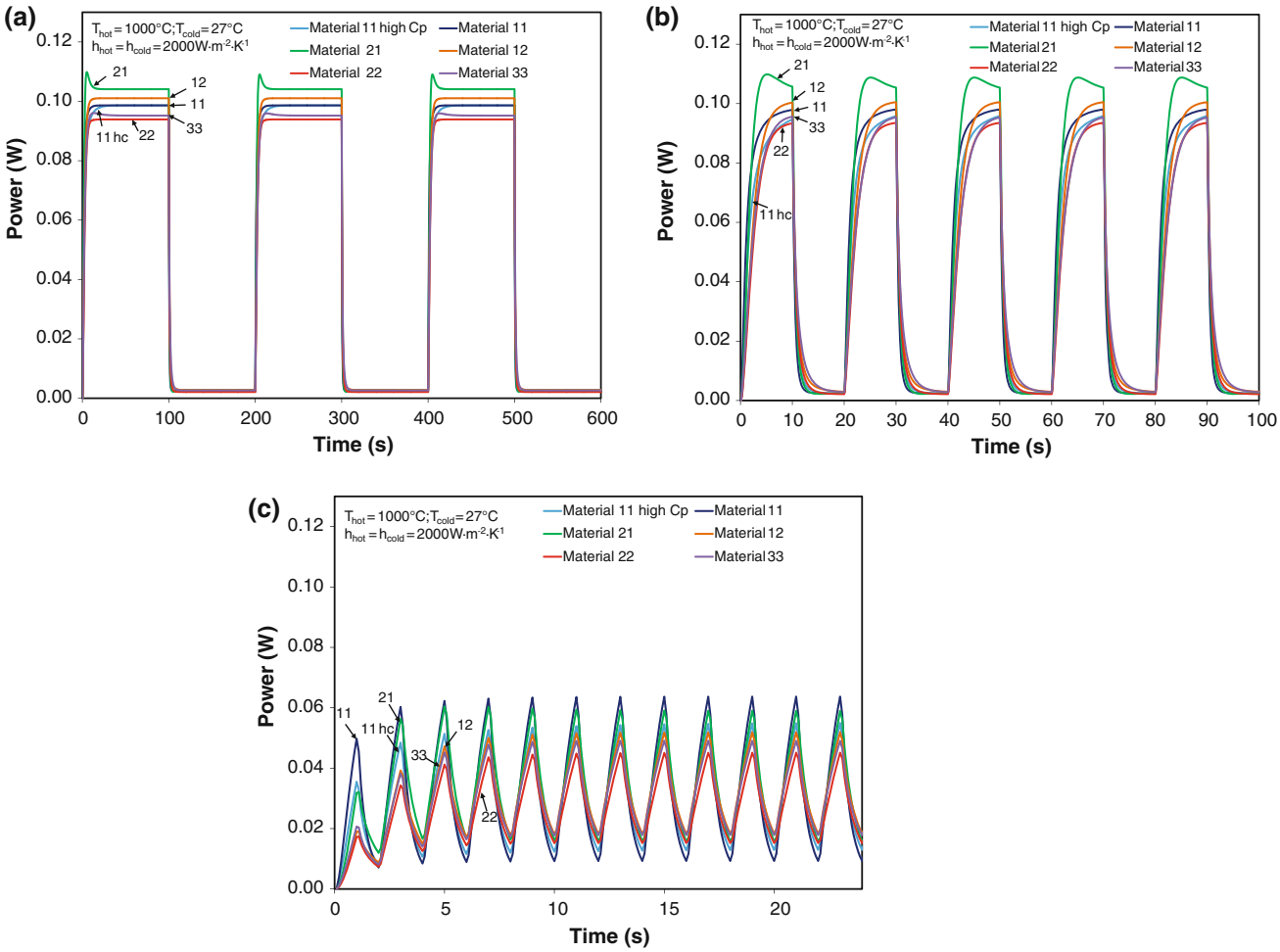

Fig. 9. Output power for cycling between 200°C and 1000°C with cycle duration of (a) 100 s, (b) 10 s, and (c) 1 s.

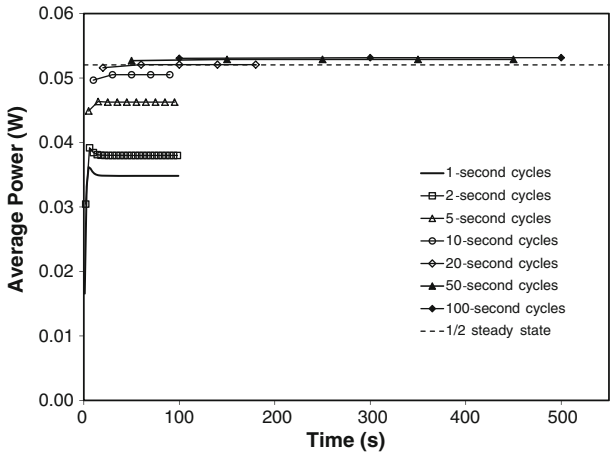

Fig. 10. Average output power over each cycle.

material 12 because the thermal conductivity of material 2 increases with increasing temperature (Fig. 1c) and material 2 is at a higher temperature in material 21. Use of a higher heat capacity for material 3 (materials 33 and 11, high C_p) extends the time required to reach the steady-state heat flux.

One measure of the efficiency of thermoelectric energy conversion (eff) is the ratio of the output power (P) to the heat entering the device (Q_{in}) according to Eq. 6, which is shown in Fig. 11c

$$\text{eff} = \frac{P}{Q_{in}}. \tag{6}$$

Since the heat transfer coefficient was selected such that the output powers are similar, the materials with the highest heat flux have the lowest efficiencies according to this metric. The broken lines represent the efficiencies calculated from the steady-state values of power and heat flux. These steady-state efficiencies are higher than the efficiencies from cycling since they do not include the low efficiencies during heating.

The net heat flux was determined by subtracting the heat leaving the device on the cold side from the heat entering the device on the hot side. As shown in Fig. 11d, the net heat flux reaches a constant

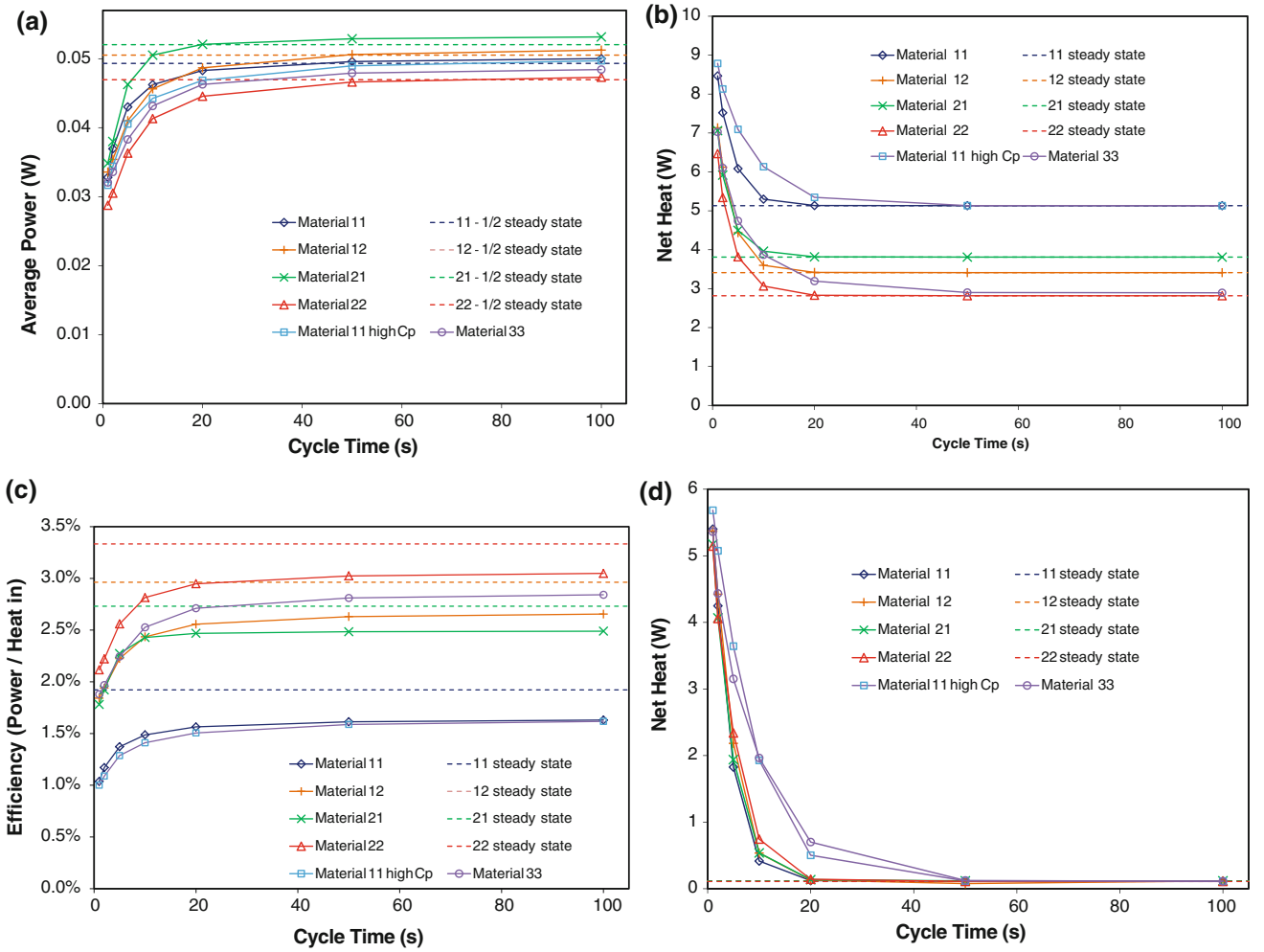

Fig. 11. Effect of cycle length on performance at steady state (last cycle): (a) power, (b) heat into device, (c) efficiency, and (d) net heat (heat into hot side–heat out of cold side).

value, and 86% to 88% of this steady-state net heat flux is converted to electricity. The cycle time length to reach the steady-state heat flux is determined by heat capacity rather than thermal conductivity, since material 11 with high C_p takes the same cycle length time as material 33 to reach the steady-state net heat flux even though the thermal conductivity of material 1 is much higher than that of material 3.

The improvement in performance by using two different materials rather than a single material is illustrated in Fig. 12, in which the results from combinations of two materials (materials 12, 21, 13, and 31) are compared with the corresponding single materials. As a conservative estimate, for each cycle length, the two-material combinations are compared with the maximum of the corresponding single materials (e.g., the results for materials 12 and 21 are compared with the maximum results from materials 1 and 2). The maximum improvement is

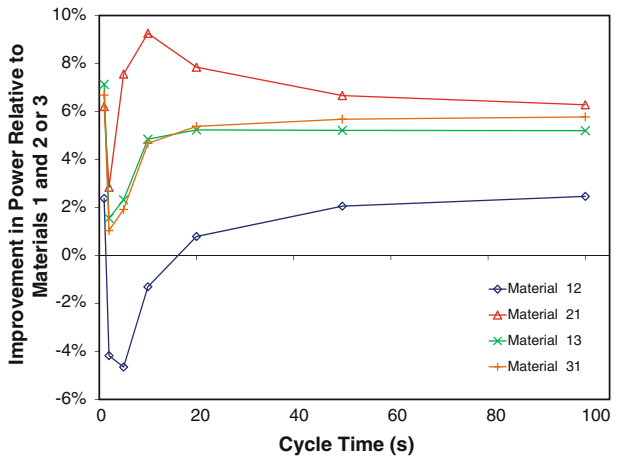

Fig. 12. Improvement in power output using two different materials (materials 12, 21, 13, and 31) relative to that using a single material (maximum power of material 1 and 2 or of material 1 and 3).

for material 21 with a 10-s cycle, but when then same two materials are reversed in position (i.e., material 12) there is no improvement for 10-s cycles and only a small improvement for longer cycles. On the other hand, the powers generated by materials 13 and 31 are similar to each other and higher than those generated by either material 1 or 3 for all cycle lengths. Although the improvement is not as great as that for material 21, the output powers for materials 13 and 31 are 5% to 6% higher than those for materials 1 and 3, and, as shown above for material 2, the addition of material 3 to material 1 increases the power even though material 3 alone generates less power than material 1.

CONCLUSIONS

Selection of materials for thermoelectric energy conversion is more complicated than comparing the traditional thermoelectric figures of merit (ZT). The relative importance of thermal and electrical conductivity depends on the operational parameters and performance objectives. In addition, the power produced by the same materials with the same figures of merit depends on the arrangement of those materials within the device. This difference can be increased under transient conditions due to variations in the temperature gradients and resulting voltages and currents. Although the benefits of using multiple materials must be evaluated considering the additional cost and complication of the additional interface and fabrication steps, strategic placement of materials in the design of the device can be used to make most effective use of the available materials.

ACKNOWLEDGEMENT

Support from the Air Force Office of Scientific Research through the Air Force Summer Faculty Fellowship Program is gratefully acknowledged.

REFERENCES

1. A.R. Knox, J. Buckle, J. Siviter, A. Montecucco, and E. McCulloch, *J. Electron. Mater.* 42, 1807 (2013).
2. T. Terayama, S. Nagata, Y. Tanaka, A. Momma, T. Kato, M. Kunii, and A. Yamamoto, *J. Electron. Mater.* 42, 2306 (2013).
3. Y. Meydbray, R. Singh, and Ali Shakouri, *Proc. 24th Int. Conf. Thermoelectrics* 345 (2005).
4. A. Moser, M. Erd, M. Kostic, K. Cobry, M. Kroener, and P. Woias, *J. Electron. Mater.* 41, 1653 (2012).
5. D. Crane, J. LaGrandeur, V. Jovovic, M. Ranalli, M. Adldinger, E. Poliquin, J. Dean, D. Kossakovski, B. Mazar, and C. Maranville, *J. Electron. Mater.* 42, 1582 (2013).
6. D. Tatarinov, D. Wallig, and G. Bastian, *J. Electron. Mater.* 41, 1706 (2012).
7. A. Elefsiniotis, D. Samson, Th Becker, and U. Schmid, *J. Electron. Mater.* 42, 2301 (2013).
8. R. McCarty, *J. Electron. Mater.* 42, 1504 (2013).
9. E. Sandoz-Rosado and R. Stevens, *J. Electron. Mater.* 39, 2010 (2010).
10. C. Baker, P. Vuppuluri, L. Shi, and M. Hall, *J. Electron. Mater.* 41, 1290 (2012).
11. C.Q. Su, W.W. Zhan, and S. Shen, *J. Electron. Mater.* 41, 1693 (2012).
12. G.-Y. Huang and D.-J. Yao, *J. Electron. Mater.* 42, 1982 (2013).
13. D. Nemir and J. Beck, *J. Electron. Mater.* 39, 1897 (2010).
14. G.J. Snyder, *Appl. Phys. Lett.* 84, 2436 (2004).
15. G.J. Snyder and T.S. Ursell, *Phys. Rev. Lett.* 91, 148301 (2003).
16. W. Seifert, E. Müller, and S. Walczak, *Phys. Status Solidi (a)* 205, 2908 (2008).
17. D.T. Crane, D. Kossakovski, and L.E. Bell, *J. Electron. Mater.* 38, 1382 (2009).
18. T.J. Hendricks, N.K. Karri, T.P. Hogan, and C.J. Cauchy, *J. Electron. Mater.* 42, 1725 (2013).
19. T. Yang, J. Xiao, P. Li, P. Zhai, and Q. Zhang, *J. Electron. Mater.* 40, 967 (2011).
20. M.S. El-Genk and H.H. Saber, *Energy Convers. Manag.* 44, 1069 (2003).
21. T.J. Hendricks, *J Energy Resour. Technol.* 129, 223 (2007).
22. D.T. Crane and J.W. LaGrandeur, *J. Electron. Mater.* 39, 2142 (2010).
23. N. Espinosa, M. Lazard, L. Aixala, and H. Scherrer, *J. Electron. Mater.* 39, 1446 (2010).
24. L. Zhang, T. Tosho, N. Okinaka, and T. Akiyama, *Mater. Trans.* 49, 1675 (2008).
25. T. Fujisaka, H. Sui, and R.O. Suzuki, *J. Electron. Mater.* 42, 1688 (2013).
26. M. Picard, S. Turenne, D. Vasilevskiy, and R.A. Masut, *J. Electron. Mater.* 42, 2342 (2013).
27. K. Zabrocki, E. Müller, and W. Seifert, *J. Electron. Mater.* 39, 1724 (2010).
28. J.W. Fergus, *J. Eur. Ceram. Soc.* 32, 525 (2012).
29. W.F. Goh, T.L. Yoon, and S.A. Khan, *Comput. Mater. Sci.* 60, 123 (2012).
30. R. Pässler, *J. Appl. Phys.* 110, 43530 (2011).
31. F.P. Zhang, X. Zhang, Q.M. Lu, J.X. Zhang, and Y.Q. Liu, *J. Alloys Compd.* 509, 4171 (2011).
32. D. Sedmidubský, V. Jakeš, O. Jankovský, J. Leitner, Z. Sofer, and J. Hejtmánek, *J. Solid State Chem.* 194, 199 (2012).
33. E.E. Antonova and D.C. Looman, *Proc. 24th Int. Conf. Thermoelectrics* 200 (2005).